Research Paper
Computational Methods for Differential Equations
http://cmde.tabrizu.ac.ir
Vol. *, No. *, *, pp. 1-15
DOI:10.22034/cmde.2026.69331.3411

Examining the impact of radiation through a Micro-Magneto micropolar flow on the thermal boundary layer development

Ejaz Haider Awan and Muhammad Sabeel Khan*
Department of Mathematics, Capital University of Science and Technology, 44000 Islamabad, Pakistan.

Abstract

This study presents a novel investigation into the influence of thermal radiation on the development of the thermal boundary layer in a micro-magneto-micropolar fluid flow, incorporating the effect of micromagnetorotation. For the first time in the literature, the impact of radiative heat transfer is examined in conjunction with the micromagnetorotation effect. The governing nonlinear differential equations, derived from the micropolar fluid theory and extended magnetohydrodynamic modeling with radiative heat transfer, are transformed into a system of coupled ordinary differential equations using similarity transformations. These equations are then numerically solved using the boundary value problem solver bvp4c from MATLAB. The results highlight the significant role of micromagnetorotation and radiation in modifying the velocity and temperature profiles, as well as the thermal boundary layer thickness. The interplay between rotational microstructures and thermal radiation leads to complex flow behavior that is not captured in classical models. The influence of physical parameters such as micropolar, relaxation magnetization, micromagnetorotation, radiation, Prandtl and Eckert numbers on the velocity and temperature distributions, skin friction, and Nusselt number is studied and presented. The insights gained from this study can benefit the design and thermal control of microscale devices, magnetothermal processing, and biomedical flow applications.

Keywords. Radiation effect, Micropolar flow, Magnetic flow, Micro-Magneto rotation, Numerical heat transfer.
2010 Mathematics Subject Classification. 35Qxx, 65Lxx, 76Mxx.

Uncorrected

Table 1. Nomenclature.

$\vec{V}$	Velocity vector	m/s	γ	Angular viscosity	rad/s
I	microinertia coefficient	kg/m	D	strain-rate tensor	s^{-1}
ρ	Density of fluid	kg/m^3	M	Magnetic field parameter	Wb/m^2
t	Time	s	P	Pressure	N/m^2
j	Current density	A/m^2	Ec	Eckert number	No unit
H	Applied magnetic field	Wb/m^2	β	Material parameter	No unit
M_0	Magnetization strength	A/m	ω^*	MMR parameter	No unit
H_0	Magnetic field strength	A/m	K	Micropolar parameter	m^2/Ks
ρc_p	Heat capacity	J/K	μ_o	Magnetic premeability	Tm/A
B	Magnetic induction vector	Wb/m^2	B_0	Magnetic induction strength	Wb/m^2
η	Shear viscosity	kg/ms	τ	Magnetization time relation	A/ms
η_1	Vortex viscosity	m^2/s	ϵ	Levi-Civita symbol	No unit
Rm	Relaxation magnetization parameter	No unit	Pr	Prandtl number	No unit
T	Fluid Temperature	K	W	Microrotation vector	rad/s
ω	Angular velocity	s^{-1}	Rd	Radiation parameter	No unit
MMR	Micromagnetorotation	—	MHD	Megnetohydrodynamics	—

Received: 25 September 2025; Accepted: 10 November 2026.
∗ Corresponding author. Email: ejazawan493@gmail.com.

1. Introduction

Micropolar fluids are complex fluids with microstructure and micro-rotational effects. Unlike conventional Newtonian fluids, micropolar fluids consist of hard or malleable particles that can rotate independently of the macroscopic translations. The governing equations of micropolar fluids can be used to describe a variety of real-world fluids, including blood flow, liquid crystals, and polymeric suspensions; all this is due to the characteristics that allow an extra degree of freedom. The theory of micropolar fluids was first introduced by Eringen [9] in 1966 as an extension of classical fluid mechanics that accounts for micro-rotational effects. Micropolar fluids within magnetohydrodynamics (MHD) consideration is of great interest in the literature because of their applications in large industrial fields. This theory finds its application in technical and industrial fields, including nuclear fuels, cancer treatment, blood flow devices, MHD generators, flow monitoring, and accelerated pumps. Moreover, it also finds it applications in plasma physics, geophysics, astrophysics, and missile technology, biomedical industry, glass making, fire prevention, nuclear reactor safety, furnace design, energy transformation devices, turbid water bodies, coal fired by open combustion and natural gas, photochemical reactors, naturally convectional cavities, and chemical engineering.

In the literature, a number of research articles have discussed these directions using modeling the flwo dynamics with micropolar MHD models. For instance, Ibrahim1 et al. [14] quantitatively analyzed a continuous two-dimensional flow of an electrically conducting micropolar fluid across a stretched surface to determine the effects of heat radiation. Ghonaim et al. [1] have studied the vortex viscosity, micropolar and radiation on porous plates. The impacts of skin friction and velocity profile on radiation have been discussed by Reddy et al. [24], who have also discussed the outcomes of radiation over micropolar flow within porous media. Khan et al. [15] investigated the time relaxation features for heat flux can be addressed by using a recently suggested hyperbolic heat flux equation to the MHD micropolar flow. The goal is to combine thermal radiation with microstructural effects within Maxwell fluid. Mandal et al. [20] discussed how boundary layer flow of a micropolar fluid over stretched sheet by nonlinear convection. Zubi et al. [3] examined the Darcy-Forchheimer law-based bio-convective flow behavior of a micropolar fluid across a curved stretching surface. Additionally, the stratification conditions are gained by the stretching surface's boundary. Waini et al. [30] examined the impact of thermal radiation across a sheet that contains hybrid nanoparticles. The partial differential equations are converted into equations of a specific form by implementing suitable similarity variables. The bvp4c function is then used to solve these equations. The results show that when thermal radiation is added to the flow by raising the temperature, heat transfer decreases. From a physical standpoint, increasing values indicate that more heat energy into the flow field, which raises the fluid's temperature. Madhura et al. [19] studied the MHD micropolar flow is affected by nonlinear thermal radiation. Raza et al. [23] provided that the bioconvective micropolar flow in porous material, chemical reactions and radiation changes are assessed both theoretically and numerically. Pal et al. [22] developed a computational model to study the micropolar fluid through an upward semi-infinite plate immersed in an uniform porous material due to non-linear thermal radiation. Saha et al. [25] examined how an electromagnetohydrodynamic incompressible flow on a stretching sheet can improve mass and heat transmission. The thermal relaxing properties are examined. Brownian motion, thermophoresis, and thermal radiation effects are applied to the fundamental Buongiorno nanoparticle model with stratified boundary conditions. The energy equation includes the Joule current. Using the second rule of thermodynamics, entropy generation is also covered. In order to achieve efficient industrial outputs and engineering results, heat conduction of thermal science base fluid has lately improved. Thus, the purpose is to ascertain the impacts of slip effects and heat radiation on a micropolar nanofluid over an expanding sheet close to a stagnation point. This work was conducted by Gammer et al. [10]. Madhura et al. [18] studied the behavior of nonlinear thermal radiation within micropolar flow past vertical plate. Joule heating effects, magnetic field, and viscous dissipation were considered. To examine the model, the equations are reformulated and presented the non-dimensional form using the proper dimensionless values. Kiyani et al. [17] discussed the effects of radiation on micropolar flow through a stretching sheet. The Buongiorno model under consideration includes thermophoresis and Brownian movement. Thermal radiation and dissipation features are used to study heat transmission. The inclusion of the porous medium phrase captures the effects of Darcy. Gopal [12] examined the thermal radiation effect on the micropolar fluid with constant mass and heat flows by substituted a convective boundary condition for temperature conditions for instance a constant surface temperature or constant heat flux. For fluids flowing at high

Uncorrected Proof

speeds, Joule heating, thermal diffusion, and viscous dissipation have all been analyzed. Gupta [13] discussed non linear problems in micropolar fluid flows. Venkateswarlu et al. [29] discussed numerical analysis of radiation on unsteady MHD boundary layer flow in order to examine heat and mass transport over a sheet with micropolar fluid. Sheri et al. [26] studied the impacts of Hall current in MHD, micropolar flow via a semi-infinite plate. The relevant fluid flow equations have been developed by the Boussinesq approximation. Gangadhar et al. [11] explained a theoretical investigation of temperature-dependent slip flow and thermal radiation in two-dimensional micropolar fluid through a stretched sheet. Nwabuzor et al. [21] studied the MHD micropolar flow in a porous medium, which is caused by radiation. Thirupathi et al. [27] investigated the micropolar fluid's flow across a sheet. This analysis considered the impacts of heat, viscous dissipation, and MHD. Bhargava et al. [7] studied at heat transmission and micropolar fluid flow via stretching sheet, including radiation effect. Varatharaj et al. [28] investigated the affects of micropolar fluid within porous media. Linear thermal radiation results in a discernible inaccuracy at temperature change extremes. Nonlinear thermal radiation can be used to rectify these issues. Dharmaiah et al. [8] examined the impact of radiation with non-uniform intensity source and a permeable medium on an MHD blended convective micropolar liquid over an extended sheet subject to Joule heating. Agrawal et al. [2] investigated the features of convective boundary conditions in the presence of mass transport, double-diffusive heat transfer and chemical reactions. In all these studies the impact of micromagnetorotation (MMR) [4–6] is not studied in the presence of radiative heat flux. Studying MMR with radiation heat transfer is vital to accurately model, predict, and control the behavior of modern fluids in extreme, high-tech, or miniaturized environments. It ensures safety, efficiency, and innovation in several critical applications. This article aims to study this gap in the literature. The gap due to MMR typically refers to an energy or mechanical gap that emerges in micromorphic or microstructured magnetic materials as a result of the interaction between magnetic fields and microrotation—that is, the localized rotation of magnetic or material microelements such as microdomains or nanoparticles. This effect is particularly significant within the framework of MMR in continuum mechanics. In advanced continuum theories like Cosserat theory or micromorphic elasticity, materials are capable of undergoing microrotations in addition to standard deformations such as translation and stretching. These microrotations can interact with magnetic fields, especially in magnetoactive or ferromagnetic materials possessing internal microstructures. Here, we investigate the impact of MMR in the presence of radiative heat transfer. To this end, we employ the theory of micropolar magnetic fluids with MMR effect and derive a thermal heat transfer model in PDEs which afterwards transformed into system of coupled ODEs through similarity transformations for thermal boundary layer analysis. To the best of author's knowledge, this study is first of its kind to incorporate the MMR effect within thermal radiative heat flow.

The rest of the article is organized as follows. In section 2, the mathematical model is derived and the flow assumptions are described. In section 3, the numerical method of solution is detailed. In section 4, numerical results are presented and discussed in detail. Finally, conclusions are drawn in section 5.

2. MMR heat transfer model and flow description

Consider a two-dimensional incompressible micropolar nanofluid flow over a stretching surface as shown in Fig. 1, subjected to an applied magnetic field $\overrightarrow{H} = (0, 0, H_0)$. Assume that the linear velocity, vorticity, and microrotation fields are given as $\overrightarrow{V} = (u_1, 0, u_3)$, $\overrightarrow{w} = (0, w, 0)$, and $W = (0, w_2, 0)$, respectively. The governing MMR flow dynamics is described by the following [16] set of partial differential equations.

$$\nabla.\overrightarrow{V} = 0, \tag{2.1}$$

$$\rho\frac{d\overrightarrow{V}}{dt} = -\nabla P + \eta\nabla^2\overrightarrow{V} + \nabla\times 2\eta_1(\overrightarrow{W} - \overrightarrow{\omega}) + J\times\overrightarrow{B} + (\overrightarrow{M}.\nabla)\overrightarrow{H} + \overrightarrow{M}\times(\nabla\times\overrightarrow{H}), \tag{2.2}$$

$$I\frac{d\overrightarrow{W}}{dt} = \gamma\nabla^2\overrightarrow{W} - 4\eta_1(\overrightarrow{W} - \overrightarrow{\omega}) + \overrightarrow{M}\times\overrightarrow{H}, \tag{2.3}$$

$$\begin{aligned}\rho C_p\frac{dT}{dt} &= k\nabla^2 T + \eta_2(trD^{(v)}) + 2\eta D^{(v)} : D^{(v)} + 4\eta_1(\overrightarrow{W} - \overrightarrow{\omega})^2 + \alpha tr(\nabla\overrightarrow{W})\\ &\quad + \beta(\nabla\overrightarrow{W})^T : \nabla\overrightarrow{W} + \gamma\nabla\overrightarrow{W} : \nabla\overrightarrow{W} + \tau\frac{M_0}{\overline{H}}(\overrightarrow{W}\times\overrightarrow{H})^2 + \nabla q_r,\end{aligned} \tag{2.4}$$

Uncorrected Proof

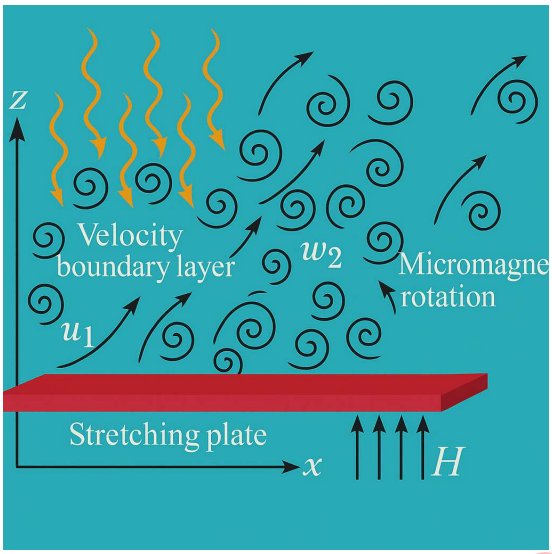


FIGURE 1. Schematic of the MMR flow and configuration.

Uncorrected Proof

where, in Eqs. (2.1)-(2.4), $\overrightarrow{V}$, $\overrightarrow{H}$, P,$\overrightarrow{w}$, $\mathbf{W}$, I, M, M_0, T, and $\overrightarrow{B}$ are the velocity field vector, magnetic induction vector, pressure field, angular velocity, micro-rotation velocity, microinertia coefficient, magnetization vector, magnetization strength, tensor matrix, and magnetic field, respectively. In Eq. (2.2), J is the current density defined as

$$J = \sigma(\overrightarrow{E} + \overrightarrow{V} \times \overrightarrow{B}), \tag{2.5}$$

where $\overrightarrow{E}$ is the electric field intensity and $\overrightarrow{B}$ is the magnetic field given by

$$\overrightarrow{B} = \mu_0 \overrightarrow{H} + \overrightarrow{M}, \tag{2.6}$$

where,

$$\overrightarrow{M} = \frac{M_0(I - \tau\overrightarrow{W}.\epsilon).\overrightarrow{H}}{\overline{H}}. \tag{2.7}$$

In Eq. (2.7) ϵ is the third order permutation tensor. The parameters η, η_1, and γ are shear viscosity, vortex velocity, and angular viscosity, respectively. Furthermore, α, β, are spin viscosities, $D^{(v)}$, τ, T, $\overline{H}$ are strain-rate tensor, relaxation time of magnetization, temperature field and magnitude of magnetic field vector respectively. The terms $\overrightarrow{M} \times \overrightarrow{H}$ in Eq. (2.3) and $\tau\frac{M_o}{\overline{H}}(\overrightarrow{W} \times \overrightarrow{H})^2$ in Eq. (2.4) are due to MMR, which specifies the influence of magnetization on microrotation at temperature. The last term in Eq. (2.4) is due to the radiative heat flux. The Rosseland's relation for q_r is given [15] by is given by

$$q_r = -\frac{4\sigma^*}{3k^*}\frac{\partial T^4}{\partial z} = -\frac{16\sigma^* T_\infty^3}{3k^*}\frac{\partial T}{\partial z}. \tag{2.8}$$

Here, k^* describes the mean absorption coefficient and σ^* is the Stefan-Boltzmann constant. The quantity ω in Eqs. (2.2)-(2.4), defined as

$$\overrightarrow{w} = \nabla \times \frac{\overrightarrow{V}}{2}. \tag{2.9}$$

represents the angular velocity of the bulk fluid and is equal to one-half of the vorticity vector. Physically, it describes the rate at which an infinitesimal fluid element rotates as it moves with the flow due to the macroscopic velocity field. In micropolar fluid theory, ω is distinct from the microrotation vector $\overrightarrow{W}$, which represents the independent rotation of the fluid microelements or suspended nanoparticles. The difference $\overrightarrow{W} - \omega$ quantifies the relative rotation between

the microelements and the surrounding fluid, and this relative motion generates the spin-coupling torque through the vortex viscosity η_1. When $\overrightarrow{W}$=ω, the microelements rotate synchronously with the fluid, and the coupling torque vanishes.

The strain-rate tensor $\mathbf{D}^{(v)}$ in Eq. (2.4) is defined as

$$\mathbf{D}^{(v)} = \frac{1}{2}\Big(\nabla\overrightarrow{V} + (\nabla\overrightarrow{V})^T\Big). \tag{2.10}$$

After the assumptions mentioned before the component form of Eqs. (2.1)-(2.4) are expressed as

$$\frac{\partial u_1}{\partial x} + \frac{\partial u_3}{\partial z} = 0, \tag{2.11}$$

$$\rho\left(u_1\frac{\partial u_1}{\partial x} + u_3\frac{\partial u_1}{\partial z}\right) = -\frac{\partial p}{\partial x} + J_yB_z + \eta\left(\frac{\partial^2 u_1}{\partial x^2} + \frac{\partial^2 u_1}{\partial z^2}\right) + M_1\frac{\partial H_1}{\partial x} + M_3\frac{\partial H_3}{\partial x} - 2\eta_1\left(\frac{\partial w_2}{\partial z} - \frac{1}{2}\left(\frac{\partial^2 u_1}{\partial z^2} - \frac{\partial u_3}{\partial z\partial x}\right)\right), \tag{2.12}$$

$$\rho\left(u_1\frac{\partial u_3}{\partial x} + u_3\frac{\partial u_3}{\partial z}\right) = -\frac{\partial p}{\partial z} + J_yB_x + \eta\left(\frac{\partial^2 u_3}{\partial x^2} + \frac{\partial^2 u_3}{\partial z^2}\right) - M_1\frac{\partial H_1}{\partial z} - M_3\frac{\partial H_3}{\partial z} + 2\eta_1\left(\frac{\partial w_2}{\partial x} + \frac{1}{2}\left(\frac{\partial^2 u_3}{\partial x^2} - \frac{\partial u_1}{\partial z\partial x}\right)\right), \tag{2.13}$$

$$u_1\frac{\partial w_2}{\partial x} + u_3\frac{\partial w_2}{\partial z} = \gamma\left(\frac{\partial^2 w_2}{\partial x^2} + \frac{\partial^2 w_2}{\partial z^2}\right) - 2\eta_1\left(2w_2 + \frac{\partial u_1}{\partial z} - \frac{\partial u_3}{\partial x}\right) + M_3H_1 - M_1H_3, \tag{2.14}$$

and

$$\rho c_p\left(u_1\frac{\partial T}{\partial x} + u_3\frac{\partial T}{\partial z}\right) = \kappa\left(\frac{\partial^2 T}{\partial x^2} + \frac{\partial^2 T}{\partial z^2}\right) + \eta_2\left(\frac{\partial u_1}{\partial x} + \frac{\partial u_3}{\partial z}\right) + \eta\left(2\left(\frac{\partial u_1}{\partial x}\right)^2 + \left(\frac{\partial u_1}{\partial z}\right)^2\right) + 4\eta_1\left(w_2 - \frac{1}{2}\left(\frac{\partial u_1}{\partial z}\right)\right)^2 + \gamma\left(\left(\frac{\partial w_2}{\partial x}\right)^2 + \left(\frac{\partial w_2}{\partial z}\right)^2\right) + \tau\frac{M_0}{\overline{H}}\left(w_2H_3\right)^2 - \frac{\partial q_r}{\partial z}. \tag{2.15}$$

These partial differential equations are subjected to the following boundary conditions.

$$\begin{aligned} &u_1 = U_\infty, \quad u_3 = 0, \quad W = W_0\frac{\partial u_1}{\partial z}, \quad T = T_w \quad at \quad z = 0,\\ &u_1 \to 0, \quad W \to 0, \quad T \to \infty, \quad \text{as} \quad z \to \infty, \end{aligned} \tag{2.16}$$

where, u_1, u_3 are the velocity components of the fluid in x, z directions, H_1, H_3 are the magnetic components in x, z directions, ρ and μ are the density and dynamic viscosity respectively, (ρc_p) is the specific heat capacitance of fluid, T is the fluid temperature, and κ is the effictive thermal conductivity of fluid. The current density J in Eq. (2.5) becomes

$$(j_x, j_y, j_z)^T = (0, \sigma(u_3B_x - u_1B_z, 0)^T, \tag{2.17}$$

Now, to develop an initial boundary value problem based on the description above, with focus on MMR effect, we make the following assumptions. The convective micropolar flow is assumed to be steady, incompressible, laminar in two-dimensional. Let $\overrightarrow{H} = (0, 0, H_0)$ be the applied magnetic field that is applied normal to the direction of flow. The flow field velocities are assumed $\overrightarrow{V} = (u_1, 0, u_3)$, $\overrightarrow{w} = (0, w(x, z), 0)$ and $\overrightarrow{W} = (0, w_2, 0)$. The components of the magnetization vector in Eq. (2.7) are expressed as

$$(M_x, M_y, M_z) = (\tau M_0W, 0, M_0). \tag{2.18}$$

Uncorrected Proof

The magnetic induction vector $\mathbf{B}$, is expressed in its component form as follows

$$(B_x, B_y, B-z) = (\tau M_0 W, 0, \mu_0 H_0 + M_0). \tag{2.19}$$

Under these simplifications and boundary layer approximations, the Eqs. (2.12)-(2.15) implies that

$$u_1\frac{\partial u_1}{\partial x} + u_3\frac{\partial u_1}{\partial z} = \left(\frac{\mu+\kappa}{\rho}\right)\frac{\partial^2 u_1}{\partial z^2} + \frac{\kappa}{\rho}\frac{\partial w_2}{\partial z} - \frac{\sigma}{\rho}\left(\left(\mu_0 H_0 + M_0\right)\tau M_0 u_3 W_2 + \left(\mu_0 H_0 + M_0\right)^2 u_1\right), \tag{2.20}$$

$$u_1\frac{\partial w_2}{\partial x} + u_3\frac{\partial w_2}{\partial z} = \frac{\gamma^*}{\rho j}\left(\frac{\partial^2 w_2}{\partial z^2}\right) - \frac{\kappa}{\rho j}\left(2w_2 + \frac{\partial u_1}{\partial z}\right) - \frac{\tau M_0 H_0}{\rho c} w_2, \tag{2.21}$$

and

$$\begin{aligned} u_1\frac{\partial T}{\partial x} + u_2\frac{\partial T}{\partial z} = {} & \frac{\kappa}{\rho c_p}\left(\frac{\partial^2 T}{\partial z^2}\right) + \frac{\kappa}{\rho c_p}\left(\frac{\partial u_1}{\partial x} + \frac{\partial u_3}{\partial z}\right) + \frac{\mu}{\rho c_p}\left(\frac{\partial u_1}{\partial z}\right)^2 \\ & + \frac{4\kappa}{\rho c_p}\left(w_2 - \frac{1}{2}\frac{\partial u_1}{\partial z}\right)^2 + \frac{\tau M_0 H_0^2}{\overline{H}\rho c_p} w_2^2 - \frac{1}{\rho c_p}\frac{16\sigma^* T_\infty^3}{3k^*}\frac{\partial^2 T}{\partial z^2}. \end{aligned} \tag{2.22}$$

Let us assume the following transformations

$$\begin{aligned} & \xi = z\sqrt{\frac{U_\infty}{\nu x}}, \quad \psi = U_\infty\sqrt{\frac{\nu x}{U_\infty}} f(\xi), u_1 = U_\infty f'(\xi), \quad u_3 = \frac{1}{2}\sqrt{\frac{U_\infty \nu}{x}}(\xi f'(\xi) - f(\xi)), \\ & w_2 = U_\infty\sqrt{\frac{U_\infty}{\nu x}} R(\xi), \quad \text{and} \quad \theta(\xi) = \frac{T - T_\infty}{T_w - T_\infty}. \end{aligned} \tag{2.23}$$

Using Eq. (2.23), in Eqs. (2.20)-(2.22), the following nonlinear coupled ODEs are obtained

$$(1+K)f''' + KR' - \frac{A}{2}(\xi f' - f)R + Mf' + \frac{ff''}{2} = 0, \tag{2.24}$$

$$\left(1 + \frac{K}{2}\right)R'' - \beta(2R + f'') - ww^* R + \frac{f'R}{2} + \frac{fR'}{2} = 0, \tag{2.25}$$

and

$$\frac{1}{Pr}\left(1 + \frac{4}{3}Rd\right)\theta'' + (1+K)E_c f''^2 + (4K + R_m)E_c R^2 - 4KE_c R f'' + \frac{f\theta'}{2} = 0. \tag{2.26}$$

The boundary conditions in Eq. (2.16) are transformed to

$$\begin{aligned} & f = 0, \quad f' = 1, \quad R = 0, \quad \theta = 1 \quad at \quad \xi = 0, \\ & f' = 0, \quad R = 0, \quad \theta = 0, \quad as \quad \xi \to \infty. \end{aligned} \tag{2.27}$$

Here, the parameters K, ξ, β, w, M, A, $w*$, R_m, Pr and Ec are dimensionless and are stated as follows.

$$\begin{aligned} & K = \frac{k}{\mu}, \quad \xi = \frac{H_0^2}{c^2 l}, \quad \left(1 + \frac{k}{2}\right) = \frac{\gamma^*}{\rho j}, \quad \beta = \frac{k}{\rho j}, M = \frac{\sigma}{\rho}\frac{B_0^2}{c}, \quad w* = \frac{\tau}{c}, \\ & w = \frac{M_0 H_0^2}{\rho\overline{H}}, \quad R_m = \frac{\tau M_0 H_0^2}{\mu\overline{H}}, \quad A = \frac{\sigma}{\rho}(\mu_0 H_0 + M_0)\tau M_0, \quad Pr = \frac{\mu C_p}{k}, \\ & E_c = \frac{U_\infty^2}{C_p(T_w - T_\infty)}, \quad \text{and} \quad Rd = \frac{4\sigma^* T_\infty^3}{\kappa\kappa^*}. \end{aligned} \tag{2.28}$$

Uncorrected Proof

The parameter of physical interest is the skin-friction coefficient and the Nusselt number. The skin-friction coefficient is defined as

$$C_f = \frac{\tau_w}{\rho u_w^2}, \tag{2.29}$$

where $u_w = cx$ is the characteristic velocity and τ_w is the wall shear stress given by

$$\tau_w = \left[(\mu + k)\frac{\partial u_1}{\partial z} + kW\right]_{z=0}. \tag{2.30}$$

Substituting Eq. (2.28) into Eq. (2.30), the skin friction coefficient in Eq. (2.29) takes the following form

$$C_f\sqrt{Re_x} = (1+K)f''(0) + KR(0). \tag{2.31}$$

The Nusselt number is defined by

$$Nu_x = \frac{xq_w}{k(T_w - T_\infty)}, \tag{2.32}$$

where the wall heat flux is given by

$$q_w = -k\frac{\partial T}{\partial z}. \tag{2.33}$$

By using Eq. (2.33) into Eq. (2.32), the Nusselt number takes the following form

$$(Re_x)^{-1/2}\, Nu_x = -\Big(1 + \frac{4}{3}Rd\Big)\theta', \tag{2.34}$$

where, $Re_x = \dfrac{u_w x}{\nu}$, is the local Reynold's number.

3. Method of solution

The developed initial-boundary value problem in Eqs. (2.24)-(2.26) is solved numerically by the application of bvp4c. The bvp4c solver in MATLAB is based on a collocation method tailored for boundary value problems involving ordinary differential equations, utilizing the three-stage Lobatto IIIa formula to ensure fourth-order convergence. For detailed discussion on the methodology, the set of ordinary differential equations (ODEs) in Eqs. (2.24)-(2.26) are first transformed into the following system of first-order ODEs.

$$\begin{cases} y_1' = y_2, & y_1(0) = 0, \\ y_2' = y_3, & y_2(0) = 1, \\ y_3' = \left(\dfrac{1}{1+k}\right)\left(\dfrac{A}{2}(\xi y_2 - y_1)y_4 - My_2 - \dfrac{y_1 y_3}{2} - Ky_5\right), & y_3(0) = r, \\ y_4' = y_5, & y_4(0) = 0, \\ y_5' = \left(\dfrac{2}{2+k}\right)\left(\beta(2y_4 + y_3) + \omega\omega^* y_4 - \dfrac{y_2 y_4}{2} - \dfrac{y_1 y_5}{2}\right), & y_5(0) = s, \\ y_6' = y_7, & y_6(0) = 1, \\ y_7' = Pr\left(\dfrac{3}{3+4Rd}\right)\left(4KEcy_4y_3 - (1+K)Ecy_3^2 - (4K+Rm)Ecy_4^2 - \dfrac{y_1 y_7}{2}\right), & y_7(0) = t. \end{cases} \tag{3.1}$$

The domain is splited into 1000 linear elements. This system is then solved together with bvp4c. Computational domain is chosen to be [0, 4] instead of the infinite domain [0,∞], this is due to the attainment of the boundary layer development. For the validation of the results obtained through this implementation the model problem is solved using MATLAB solver. The collocation technique and a point mesh are used to divide the integration interval into smaller intervals. To validate the accuracy of the obtained solutions, skin-friction coefficient is computed with bp4c and shooting methods against the material parameters Rd, Rm, K, A and β, with varying values of the MMR parameter ω^*. The Table 1, displays the calculated solutions in relation to the skin-friction coefficient. These calculations show that the skin-friction coefficient values obtained are in srtong agreement with the values from the shooting method.

Uncorrected Proof

TABLE 2. Skin-friction coefficient $C_f\sqrt{Re_x}$ for varying physical parameters.

K	A	β	ω^*	Skin-friction
0	0.5	0.5	0.5	0.111804
0.5				0.250988
1.0				0.389736
1.5				0.528259
	0.0			0.109009
	0.1			0.109937
	0.2			0.110595
		0		0.111804
		2.0		0.111804
		4.0		0.074386
			1.5	0.111804
			2.5	0.111804
			3.5	0.111804

4. RESULTS AND DISCUSSIONS

In this section, numerical results are presented for the MMR initial boundary value problem in Eqs. (2.24)-(2.26). Numerical experiments are performed for different values of the material parameters to calculate the translational, rotational velocity profiles and temperature profiles in micropolar cases. A thorough discussion on the Table 1 has been conducted which contains the impact of dimensionless parameters K, A, β and ω^* on the skin friction coefficient. For the rising values of K and β, skin friction is directly propotional to the β and inversely propotional to the K. Table 2 explains the impacts of K, Rm, Ec , Pr and Rd on the Nusselt number. Figure 2 shows the impact of magnetization

Proof

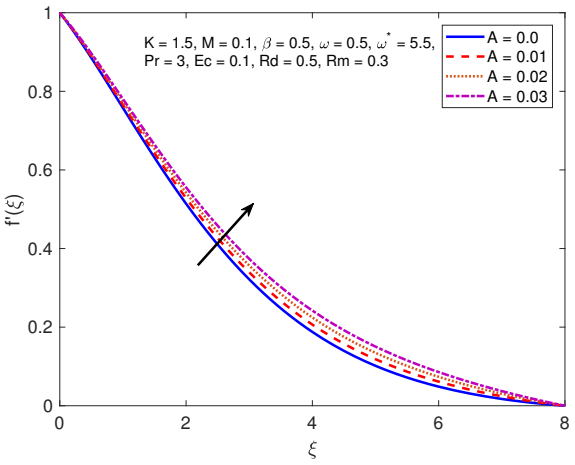


FIGURE 2. Translational velocity profile for varying values of A.

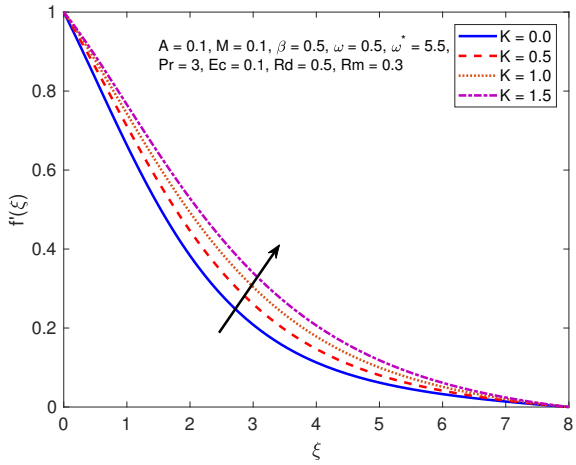


FIGURE 3. Translational velocity profile for varying values of K.

parameter A on the translational velocity profile. The rise in the values of magnetization parameter results in an increase in the profile of translational velocity. The value of magnetization parameter seems to describe the effect of magnetic fields and magnetization dynamics on the fluid behavior, especially when there is substantial electrical and magnetic conduction. With an increase in micropolar parameter K, the translational velocity tends to increase. This is so that translational motion is resisted by increased couple stresses, which increase internal friction in the fluid.

TABLE 3. Nusselt number Nu for varying physical parameters.

K	R_m	Ec	β	Pr	Rd	Nusselt number
1.3	0.5	0.1	1.0	0.3	0.5	0.327834
1.7						0.305859
2.0						0.296394
2.5						0.286149
	1					0.296636
	1.5					0.296878
	2.0					0.297120
	2.5					0.297362
		0.3				0.323021
		0.5				0.348679
		0.7				0.374337
		0.9				0.399996
			1.5			0.440681
			2.0			0.478766
			2.5			0.513903
			3.0			0.546152
				1.3		1.487420
				2.3		2.193770
				3.3		2.800850
				4.3		3.346920
					1.5	2.402090
					2.5	2.096350
					3.5	1.947920
					4.5	1.860720

Uncorrected Proof

With an increase in micropolar parameter, the translational velocity tends to increase. This is so that translational motion is resisted by increased couple stresses, which increase internal friction in the fluid. Higher couple stresses cause the fluid to become more resistant to flow, which slows down translational velocity. The physical behavior of velocity profiles versus variations in micropolar parameter is depicted in Figure 3. The fluid's velocity increases as the intensity in micropolar parameter increases, as seen by the graph.

The impacts of the magnetic field parameter M on the translational velocity profiles for the Newtonian and non-Newtonian scenarios are shown in Figure 4. It is seen that the fluid velocity increased in tandem with micropolar parameter. Thus, a Lorentz force decreases the velocity field. Physically speaking, as the magnetic field becomes stronger and the Lorentz force rises. The material parameter β impacts on the fluid's macroscopic flow and thermal behavior interact with its microstructural features. In Figure 5, the influence of material parameter on translational velocity profile is observed. we can see clearly that translational velocity profile will decline with the rise of values of material parameter.

The MMR parameter is an idea that can develop during research on materials or fluids driven by both micro-rotation effects and magnetic fields. In general, this property depicts the small-scale rotational effects, or microrotation, that are impacted by a magnetic field. In such systems, the translational velocity, rotational velocity and temperature profiles are largely determined by the MMR parameter. Figure 6 represents how MMR affects the translational velocity profile. The velocity profile shows an increase with incrementing the MMR parameter. Figure 7 displays the impact of A on the rotational velocity profile. The effect of magnetization on boundary layer profiles is observable in a specific pattern in the vicinity of the stretching surface relative to the distant vicinity. The observed patterns in the boundary layer profiles can be affected by various factors, such as fluid's characteristics, the geometry of the flow,

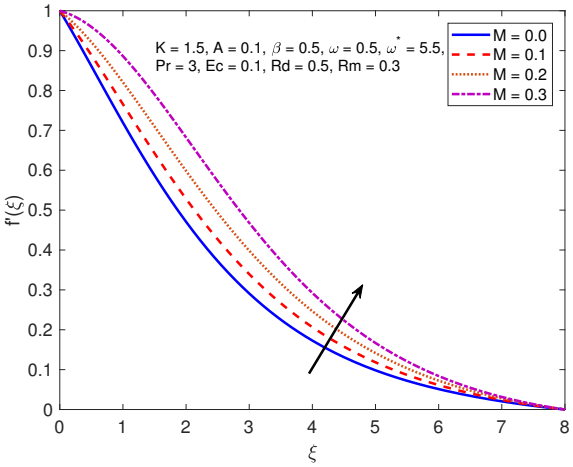


FIGURE 4. Translational velocity profile for varying values of M.

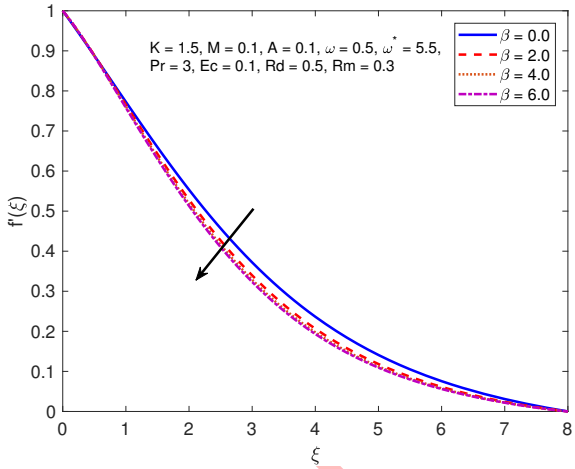


FIGURE 5. Translational velocity profile for varying values of β.

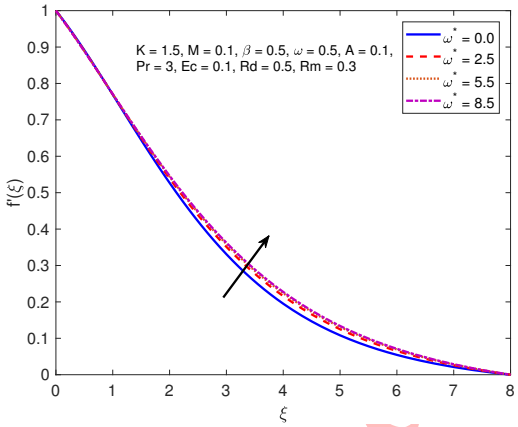


FIGURE 6. Translational velocity profile for varying values of ω^*.

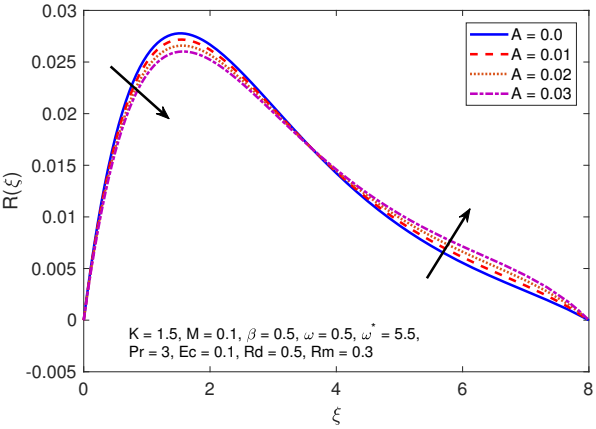


FIGURE 7. Rotional velocity profile for varying values of A.

and the strength of the magnetic field. The velocity profiles show a trend to decrease in the vicinity of the stretching surface and increase in the boundary layer region.

With an increase in micropolar parameter, the translational velocity tends to decrease near the wall of sheet and high with boundary layer regions. This is so that rotational motion is resisted by increased couple stresses, which increase internal friction in the fluid. Higher couple stresses cause the fluid to become more resistant to flow, which slows down translational velocity. The physical behavior of velocity profiles versus variations in micropolar parameter is depicted in Figure 8. The impacts of the magnetic field parameter on the rotational velocity profiles for the Newtonian and non-Newtonian scenarios are shown in Figure 9. It is observed that the velocity of the fluid increased in the boundary layer region and decreased near the wall with magnetic field parameter. Thus, a Lorentz force decreases the velocity field. Physically speaking, the magnetic field becomes stronger and the Lorentz force rises.

Figure 10 represents how MMR affects the rotational velocity profile. The velocity profile shows a decrease with the increment of MMR parameter. In Figure 11, the impact of material parameter on rotational velocity profile is

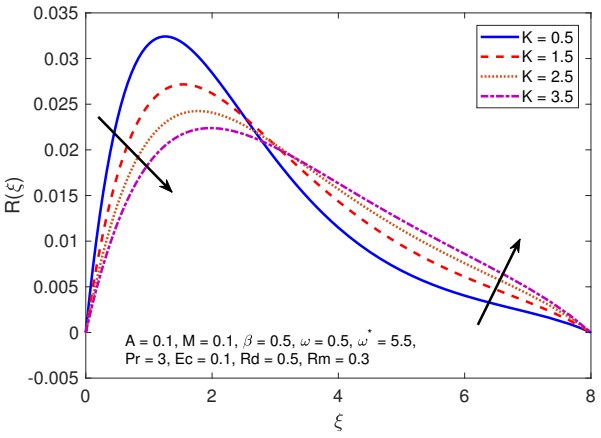


FIGURE 8. Rotational velocity profile for varying values of K.

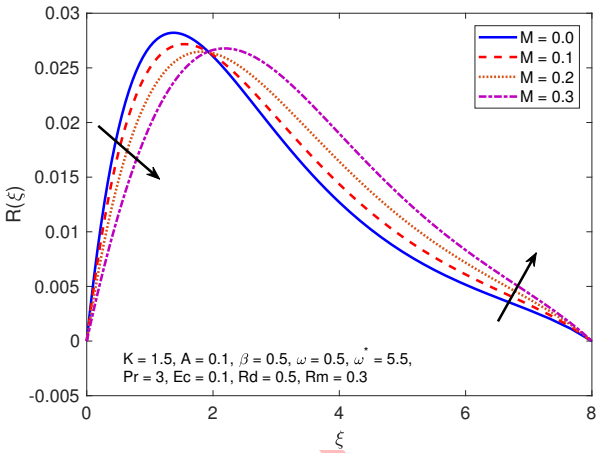


FIGURE 9. Rotational velocity profile for varying values of M.

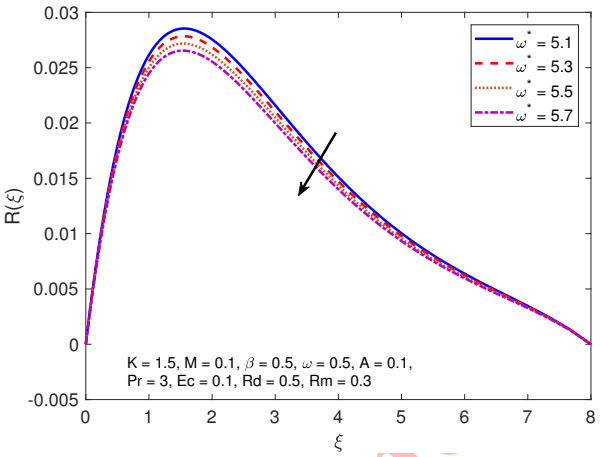


FIGURE 10. Rotational velocity profile for varying values of ω^*.

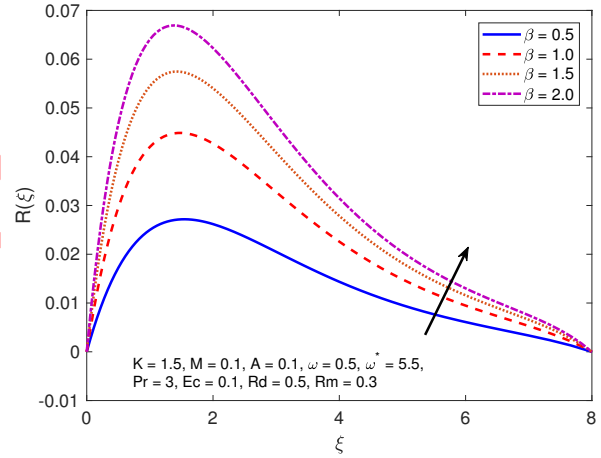


FIGURE 11. Rotational velocity profile for varying values of β.

observed. we can clearly see that the rotational velocity profile will decrease with the increase of values of material parameter.

Figure 12 displays the impact of magnetization parameter on the temperature profile. The rise in the values of A results in the decrease in the profile of temperature. With an increase in micropolar parameter, the temperature profile tends to increase. Higher couple stresses cause the fluid to become more resistant to flow, which slows down temperature profile. The physical behavior of temperature profile versus variations in micropolar parameter is depicted in Figure 13. The fluid's temperature increases as the intensity in micropolar parameter increases, as seen by the graph. Relaxation time parameter is a parameter that influences the rate at which a system back to equilibrium position after perturbed. It essentially dictates how quickly a system relaxes or adjusts to a new state.

The effects of the relaxation time parameter Rm on the temperature profile are shown in Figure 14. It is observed that the fluid temperature increased in tandem with relaxation time paramete.

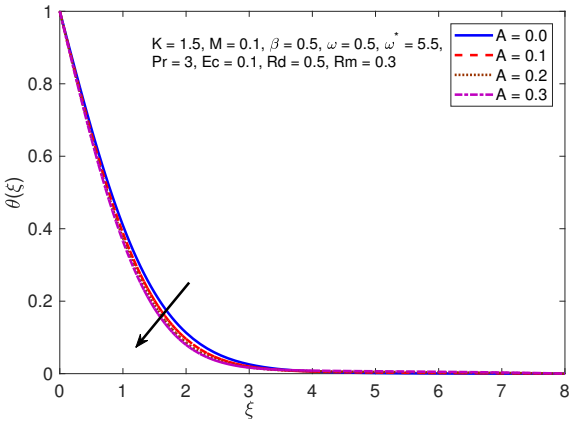


FIGURE 12. Temperature profile for varying values of A.

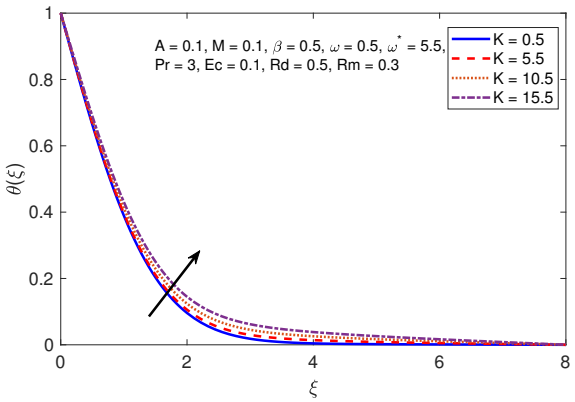


FIGURE 13. Temperature profile for varying values of K.

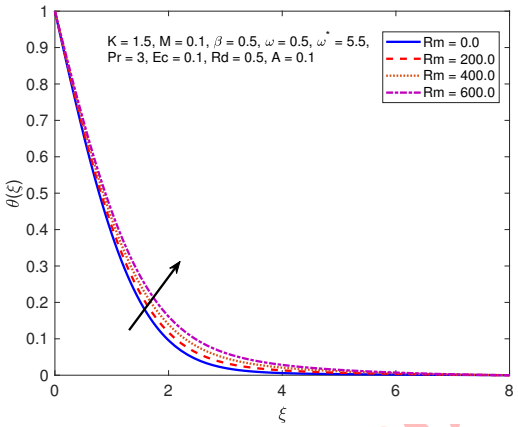


FIGURE 14. Temperature profile for varying values of Rm.

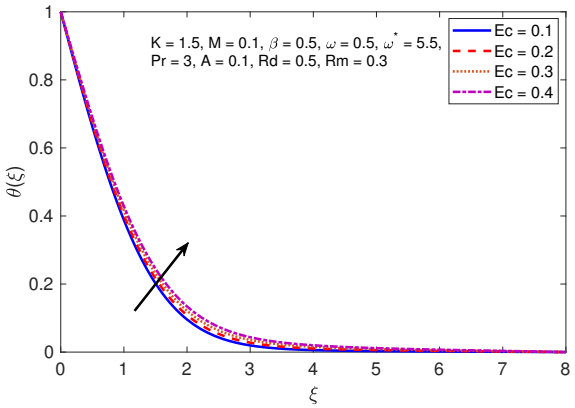


FIGURE 15. Temperature profile for varying values of Ec.

The Ekert number is a dimensionless quantity utilized in fluid mechanics and heat transport. It illustrates the relation, especially with compressible flow between the kinetic energy and enthalpy, or heat energy of a flowing fluid. The Ekert number and the temperature profile of the system are directly correlated since it considers the difference in temperature between the two points. When a system's Ekert number is high, the fluid's thermal energy and kinetic energy are equal, leading the temperature profile to vary significantly. A fluid with a high Ekert number maintains more kinetic energy than thermal energy. This usually happens in rapid flows. Sharp gradients can be seen in the temperature profile, especially in areas that are rapidly growing or compressing. Figure 15 demonstrates the impact of Ec on the temperature profile. Raising the values of Ekert number, it is clearly observed that the temperature profile is increased due to the decrement in heat transfer rate.

In fluid dynamics and heat transfer, the Prandtl number is a dimensionless quantity that is important to know the relation between the thermal diffusivity and momentum diffusivity of a fluid, also known as viscous diffusion. It is especially important to understand the development of temperature profiles in various flows. The Prandtl number has a direct impact on the temperature profile in a fluid flow, especially in boundary layer flows as momentum and heat

Uncorrected Proof

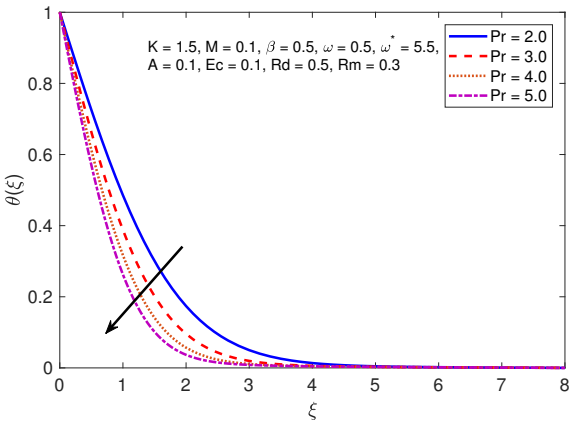


FIGURE 16. Temperature profile for varying values of Pr.

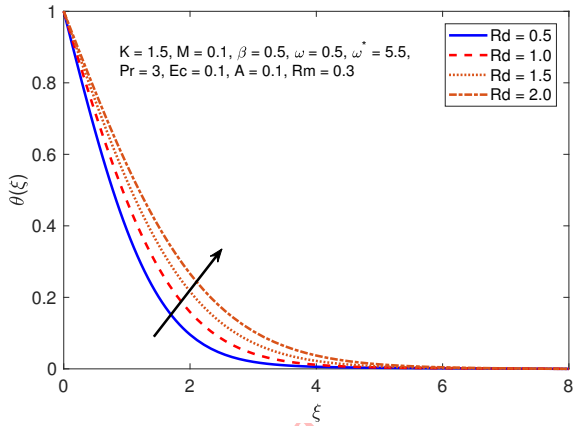


FIGURE 17. Temperature profile for varying values of Rd.

Uncorrected Proof

transfer occur simultaneously. The thermal boundary layer is thinner than the velocity boundary layer. Figure 16 shows the effects of Prandtl number on the temperature distribution. Graphs indicate that the fluid temperature decreases as Prandtl number increases in magnitude. It leads to a decline in the fluid's thermal conductivity. The temperature field decreases as the Prandtl number increases as a result of the fluid's thermal conductance being reduced. Important parametric effects on fluid temperature $\theta(\xi)$ are examined here. Figure 17 illustrates how the thermal radiation parameter Rd affects the temperature profile. It is clear that the temperature shape expands as radiation paramete values rise. Higher values of radiation paramete enhanced the heat flow from the sheet and provided more heat to the working fluid inside the boundary layer, raising the fluid's temperature, which explains this outcome.

5. Conclusion

This study has introduced a comprehensive numerical analysis of the thermal boundary layer development in micro magneto-micropolar fluid flows under the combined effects of thermal radiation and MMR. By incorporating radiative heat transfer into the extended framework of micropolar fluid theory and MHD modeling, the work presents a novel approach to understanding microscale flow behavior, particularly where internal rotational microstructures and magnetic interactions coexist.

Through the use of similarity transformations and the numerical solver bvp4c in MATLAB, the complex system of governing equations was successfully reduced and solved. The results demonstrate that both micromagnetorotation and radiation profoundly influence the velocity and temperature distributions. The presence of these effects notably alters the thermal boundary layer thickness, deviating from classical fluid models which ignore such microscale phenomena.

Parametric analysis further revealed the sensitivity of the system to key physical parameters, such as the micropolar parameter, radiation parameter, relaxation magnetization, Prandtl number, and Eckert number. These parameters significantly impact skin friction and heat transfer characteristics, highlighting the intricate balance between thermal and magnetic microscale interactions.

Overall, the findings highlight the importance of considering micromagnetorotation and radiation in the thermal analysis of microscale fluid systems. The insights gained from this investigation can inform the optimized design of thermal control systems in microdevices, magneto-thermal processing technologies, and biomedical microfluidic applications. Future studies may focus on numerical experimental validation and the inclusion of additional physical effects such as variable viscosity, slip conditions, or non-Fourier heat conduction to further extend the predictive capabilities of this model.

References

[1] E. M. Abo-Eldahab and A. F. Ghonaim, *Radiation effect on heat transfer of a micropolar fluid through a porous medium*, Appl. Math. Comput., *169*(1) (2005), 500–510.

[2] A. Agrawal and J. P. Panda, *Study the effect of thermal diffusion and viscous dissipation on MHD flow of micropolar fluid*, Int. J. Appl. Comput. Math., *11*(2) (2025), 31.

[3] M. A. Al Zubi, M. Naveed Khan, N. Ahsan, M. Hussien, K. A. Gepreel, and M. D. Albalwi, *Numerical heat transfer analysis of bio convective flow of non-Newtonian nanofluid with Darcy-Forchheimer effect over a curved stretching surface*, Numer. Heat Transf., Part A: Appl., *86* (2024), 1–17.

[4] K. E. Aslani, L. Benos, E. Tzirtzilakis, and I. E. Sarris, *Micromagnetorotation of MHD micropolar flows*, Symmetry, *12*(1) (2020), 148.

[5] K. E. Aslani and I. E. Sarris, *Effect of micromagnetorotation on magnetohydrodynamic Poiseuille micropolar flow: analytical solutions and stability analysis*, J. Fluid Mech., *920* (2021), A25.

[6] E. H. Awan and M. S. Khan, *Computational analysis of micromagnetorotation within micropolar flow through implementation in FreeFEM++*, Comput. Methods Differ. Equ., *(2026)*.

[7] R. Bhargava, R. Sharma, and O. A. Bég, *A numerical solution for the effect of radiation on micropolar flow and heat transfer past a horizontal stretching sheet through porous medium*, in: Proc. 5th IASME/WSEAS Int. Conf. Continuum Mech. (CM'10), 2010.

[8] G. Dharmaiah, D. N. Sidorov, S. Noeiaghdam, and V. P. Panov, *The influence of a non-uniform heat source/sink and Joule heating on the convective motion of a micropolar fluid in a chemically radiative MHD medium across a stretched sheet*, iPolytech J., *28*(3) (2024), 435–452.

[9] A. C. Eringen, *Theory of micropolar fluids*, J. Math. Mech., *16* (1966), 1–18.

[10] F. Gamar, M. D. Shamshuddin, M. S. Ram, S. O. Salawu, and E. O. Fatunmbi, *Exploration of thermal radiation and stagnation point in MHD micropolar nanofluid flow over a stretching sheet with Navier slip*, Numer. Heat Transf., Part A: Appl., *86* (2024), 1–13.

[11] K. Gangadhar, K. L. Narayana, P. S. Kumar, and B. R. Kumar, *MHD micropolar fluid flow over a stretching permeable sheet in the presence of thermal radiation and thermal slip flow: a numerical study*, IOP Conf. Ser.: Mater. Sci. Eng., *263*(6) (2017), 062010.

[12] R. S. Gopal, *Effect of thermal radiation and viscous dissipation on steady MHD free convection and mass transfer flow of a micropolar fluid with constant heat and mass fluxes*, Int. J. Math. Trends Technol., *52* (2017).

[13] D. Gupta, *Non-linear problems in micropolar fluid flows*, Ph.D. dissertation, 2014.

[14] S. M. Ibrahim, T. S. Reddy, and N. B. Reddy, *Thermal radiation effects on MHD free convection flow of a micropolar fluid past a stretching surface embedded in a non-Darcian porous medium*, Innov. Syst. Des. Eng., *4*(13) (2013), 1–14.

[15] S. Ibrahim, V. Kumar, and C. S. K. Raju, *Possessions of viscous dissipation on radiative MHD heat and mass transfer flow of a micropolar fluid over a porous stretching sheet with chemical reaction*, Challenges Nano Micro Scale Sci. Technol., *6*(1) (2018), 60–71.

[16] M. S. Khan, *A new thermal boundary layer analysis model in the presence of micromagnetorotation within micropolar continuum*, Multiscale Multidiscip. Model. Exp. Des., *8*(9) (2025), 387.

[17] M. Z. Kiyani, A. M. K. Abbasi, T. Muhammad, I. Ahmad, M. Waqas, and S. Riaz, *Rheology of magneto-micropolar nanoliquid toward radiative exponential surface subjected to Brownian motion, thermal radiation, thermophoresis and viscous dissipation*, Waves Random Complex Media, *35*(2) (2025), 3033–3047.

[18] K. R. Madhura, Babitha, and S. S. Iyengar, *Numerical investigation on magnetohydrodynamics boundary layer flow of micropolar Carreau nanofluid with nonlinear thermal radiation*, Int. J. Ambient Energy, *43*(1) (2022), 6224–6232.

[19] K. R. Madhura and Babitha, *Numerical study on magnetohydrodynamics micropolar Carreau nanofluid with Brownian motion and thermophoresis effect*, Int. J. Model. Simul., *45*(2) (2025), 651–664.

[20] I. C. Mandal and S. Mukhopadhyay, *Nonlinear convection in micropolar fluid flow past an exponentially stretching sheet in an exponentially moving stream with thermal radiation*, Mech. Adv. Mater. Struct., *26*(24) (2019), 2040–2046.

Uncorrected Proof

[21] P. O. Nwabuzor, A. T. Ngiangia, and E. O. Chukwuocha, *MHD flow of micropolar fluid in a porous medium provoked by heat function and radiation*, Asian J. Phys. Chem. Sci., *6*(2) (2018), 1–20.
[22] D. Pal and B. C. Das, *Combined performance of non-linear thermal radiation and chemical reaction on MHD convective heat and mass transfer of a micropolar fluid over a non-isothermal surface*, Int. J. Ambient Energy, *43*(1) (2022), 8–22.
[23] A. Raza and D. Jeong, *An efficient alternating direction implicit method for MHD micropolar fluid with chemical reaction and radiation*, J. Therm. Anal. Calorim., *150* (2025), 1–16.
[24] L. R. Reddy, M. C. Raju, G. S. S. Raju, and S. M. Ibrahim, *Chemical reaction and thermal radiation effects on MHD micropolar fluid past a stretching sheet embedded in a non-Darcian porous medium*, J. Comput. Appl. Res. Mech. Eng. (JCARME), *6*(2) (2017), 27–46.
[25] D. Saha, A. Mahanta, S. Mukhopadhyay, and S. Sengupta, *Cattaneo–Christov heat and mass flux model for electromagnetohydrodynamic (EMHD) non-Newtonian flow of Jeffrey nanofluid with nonlinear thermal radiation and stratified boundary conditions*, Waves Random Complex Media, (2023), 1–25.
[26] S. R. Sheri and M. D. Shamshuddin, *Finite element analysis on transient MHD free convective chemically reacting micropolar fluid flow past a vertical porous plate with Hall current and viscous dissipation*, Propuls. Power Res., *7*(4) (2018), 353–365.
[27] G. Thirupathi, K. Govardhan, G. Narender, S. Misra, and P. Kavitha, *Exploring the impact of thermal radiation, viscous dissipation, and magnetic field on micropolar fluid flow over a shrinking surface with velocity slip*, JP J. Heat Mass Transf., *37*(1) (2024), 1–21.
[28] K. Varatharaj and R. Tamizharasi, *Non-linear thermal radiation and heat transfer effect on MHD flow of a micropolar fluid through a porous medium*, J. Anal., *33* (2024), 121–138.
[29] S. Venkateswarlub and K. J. Lakshmic, *Effect of magnetic field and radiation on MHD heat and mass transfer of micropolar fluid over stretching sheet with Soret and Dufour effects*, Int. J. Appl. Eng. Res., *13*(12) (2018), 10991–11000.
[30] I. Waini, A. Ishak, and I. Pop, *Flow over a shrinking sheet containing hybrid nanoparticles with nonlinear thermal radiation and magnetohydrodynamic effects*, Waves Random Complex Media, *32* (2022), 1–19.

Uncorrected Proof